THE JOURNAL OF PHYSICAL CHEMISTRY A

ARTICLE

pubs.acs.org/JPCA

Role of the $^3(\pi\pi^*)$ State in Photolysis of Lumisantonin: Insight from ab Initio Studies

Xing Chen,[†,‡] Zilvinas Rinkevicius,[‡] Yi Luo,[‡] Hans Ågren,[*,‡] and Zexing Cao[*,†]

[†]Department of Chemistry and State Key Laboratory of Physical Chemistry of Solid Surfaces, College of Chemistry and Chemical Engineering, Xiamen University, Xiamen 360015, China

[‡]Theoretical Chemistry & Biology, School of Biotechnology, Royal Institute of Technology, SE-106 91 Stockholm, Sweden

ABSTRACT: The CASSCF and CASPT2 methodologies have been used to explore the potential energy surfaces of lumisantonin in the ground and low-lying triplet states along the photoisomerization pathways. Calculations indicate that the $^1(n\pi^*)$ state is the accessible low-lying singlet state with a notable oscillator strength under an excitation wavelength of 320 nm and that it can effectively decay to the $^3(\pi\pi^*)$ state through intersystem crossing in the region of minimum surface crossings with a notable spin−orbital coupling constant. The $^3(\pi\pi^*)$ state, derived from the promotion of an electron from the π-type orbital mixed with the σ orbital localized on the C—C bond in the three-membered alkyl ring to the π^* orbital of conjugation carbon atoms, plays a critical role in C—C bond cleavage. Based on the different C—C bond rupture patterns, the reaction pathways can be divided into paths A and B. Photolysis along path A arising from C1—C5 bond rupture is favorable because of the dynamic and thermodynamic preferences on the triplet excited-state PES. Path B is derived from the cleavage of the C5—C6 bond, leading first to a relatively stable species, compared to intermediate **A-INT** formed on the ground state PES. Accordingly, path B is relatively facile for the pyrolytic reaction. The present results provide a basis to interpret the experimental observations.

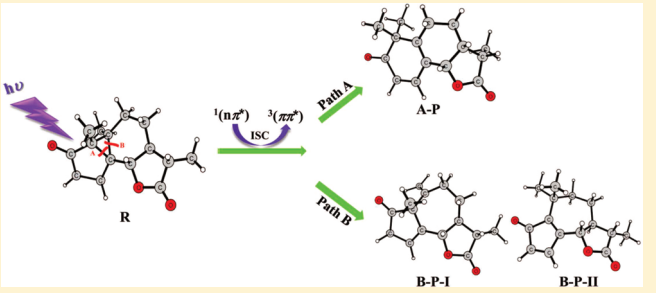

INTRODUCTION

As one of the essential photoproducts of santonin upon exposure to ultraviolet light, lumisantonin has long been systematically studied for its photochemical properties. Dating back to 1957, Arigoni and co-workers carried out a series of experiments to explore the photolysis of santonin in different media.[1] It was reported that, under UV radiation, santonin in dioxane yields lumisantonin, which, in turn, is also photoactive and undergoes a number of photoinduced reactions.[1] These findings spurred much subsequent research on the photoreaction mechanism of lumisantonin.[2−12] These studies indicated that irradiation of lumisantonin with a wavelength longer than 320 nm in an aprotic medium leads to two differential photolytic pathways, yielding two main photolytic products: The major one is mazdasantonin and its dimer, amounting to 80%, and the second is a double-bonded isomer of pyrolumisantonin, amounting to 10% of the total products.[6] The detailed mechanism proposed by Fisch and Richards in each reaction channel is schematically shown in Figure 1. Exposed to UV light, lumisantonin (**R**), featuring a three-membered alkyl ring, is promoted to an electronic excited state, immediately undergoing a bond cleavage reaction involving either the C1—C5 or C5—C6 bond; the two reaction pathways are labeled here as path A and path B, respectively. Along path A, the cleavage of the C1—C5 bond leads to an intermediate, namely, **A-INT**. A subsequent methyl migration yields a product, denoted as **A-P**. It was predicted that this reaction step takes place in the ionic-type species of **A-INT**. Along path B, breakage of the C5—C6 bond leads to an intermediate form, denoted as **B-INT**. This step followed by an intramolecular hydrogen abstraction leads to the formation of another intermediate, **B-INT-I**, with a characteristic enol configuration. It easily undergoes a ketonization reaction, where the enolic hydrogen migrates to the unconjugated β,γ-unsaturated ketone, yielding a double-bonded isomer of pyrolumisantonin, denoted as **B-P-I**.

Provided the photolysis mechanism of lumisantonin revealed from an experimental point of view mentioned above, some key problems are still to be solved. Under a given irradiation wavelength, how many excited states are involved in the photolysis, and is there any twinning along the reaction pathways? It is also important to analyze which states play leading roles in the stepwise reaction and at which point the excited state undergoes a radiationless decay to the ground state. Is it possible for the methyl group to migrate in path B? As such questions are difficult to answer by pure experimental means, theoretical calculations can be used to fill the gaps in understanding. It is the ambition of the present work to answer questions such as these at a high-accuracy computational level and to provide a profound insight into the photoreaction mechanisms of lumisantonin.

Received: April 11, 2011
Revised: May 22, 2011
Published: May 31, 2011

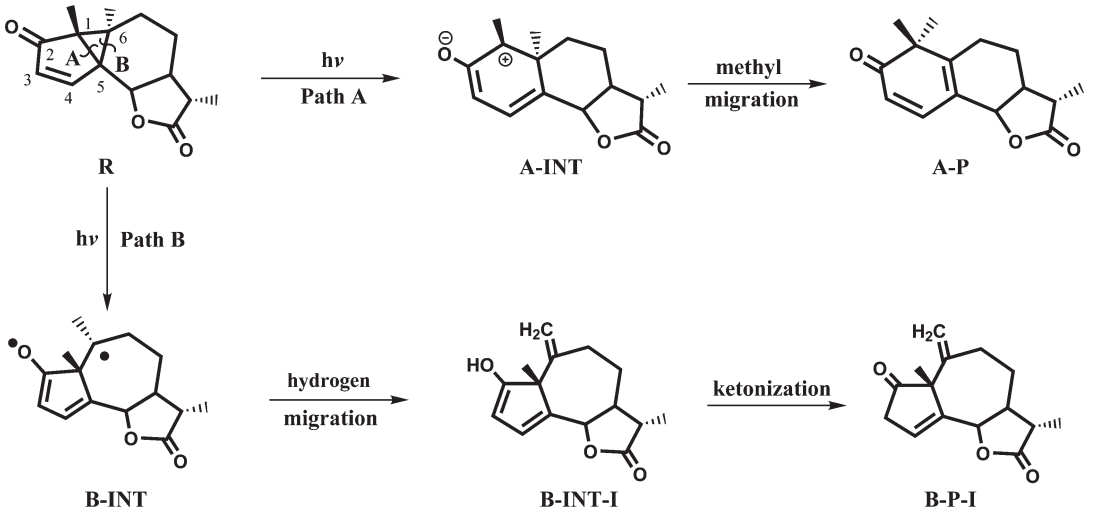

Figure 1. Experimentally suggested photoreaction pathway of lumisantonin (see ref 6).

COMPUTATIONAL DETAILS

We employed the complete-active-space self-consistent field (CASSCF)[13] with the d-polarized double split-valence 6-31G* basis set[14] to optimize the critical points along the reaction pathway. Generally, the active space involves all of the bonding and antibonding π-type orbitals, the lone pair of electrons (n-type orbital) localized on the oxygen in the reactive fragment, and the active orbitals (such as σ orbitals) relevant for the bond-breaking and bond-making process. Particularly, it consists of eight electrons distributed over seven orbitals, denoted as CASSCF(8,7). Frequency analysis of the transition state was carried out at the same level of the geometry optimization to identify whether it was a real saddle point to yield the desired product.

The vertical transition energies of the low-lying singlet excited states of lumisantonin were calculated by means of CASSCF with the d,p-polarized triple split-valence 6-311G** basis set.[15] Furthermore, the second-order multiconfigurational perturbation theory (CASPT2) methodology[16,17] was used to evaluate the energy with respect to the effect of dynamic valence-electron correlation, with an imaginary shift of 0.4 au employed to moderate the effect of intruder states in calculation.

To illustrate the photolysis mechanism of lumisantonin, the reaction pathway was constructed from all of the critical points involved in the photoreaction on the ground- and excited-state PESs. All electronic energies at the CASSCF-optimized geometries were evaluated by CASPT2 with the cc-pVDZ basis set[18] in consideration of the low computational costs and the accuracy matchable with the results given by the 6-311G** basis set. Several essential surface crossings on the nonadiabatic PESs along the reaction pathway were studied deliberately. A conical intersection as the minimum on the seam of a singlet−singlet or triplet−triplet surface crossing is responsible for an efficient radiationless, internal conversion (IC), decay channel. The energy evaluations in the CASSCF-optimized surface crossings at the CASPT2 level show that the two degenerate electronic states are split due to the dynamic valence-electron correlation at the position of the PES crossing point. The probability of an intersystem crossing (ISC) occurring on the seam of singlet−triplet surface crossings (SCs) could be estimated by calculation of the spin−orbit coupling (SOC) constant between the singlet and triplet states with a one-electron approximate spin−orbit Hamiltonian.

All optimizations of stationary points employed the Gaussian 03 program package,[19] and both the surface crossing optimizations at the CASSCF level and all energy evaluations by means of CASPT2 were carried out using Molpro 2006.[20] The SOC constants were calculated by the MOLCAS 7.4 program package.[21]

RESULTS AND DISCUSSION

Critical Points on the Photolytic Reaction Pathway. The key points on the photolytic reaction pathway were optimized at the CASSCF level; their geometries are presented in Figure 2. We carefully investigated the three low-lying excited states, namely, $^3(\pi\pi^*)$, $^3(n\pi^*)$, and $^1(n\pi^*)$, of lumisantonin in the Franck−Condon (FC) region, in accordance with the irradiation light wavelength matched to the vertical excitation energies. The evident increase of the C—O bond length by 0.138 Å in the cyclopentenone fragment in the $^1(n\pi^*)$ state at equilibrium is ascribed to the promotion of one electron from the lone pair of the n-type orbital at oxygen to the antibonding π^*-type orbital localized on the C—O bond. Marked changes take place in the C3—C4, C2—C3, C2—O, and C1—C5 bond lengths, which increase from 1.343, 1.486, 1.205, and 1.508 Å in the ground state to 1.511, 1.447, 1.237, and 1.535 Å, respectively, in the $^3(\pi\pi^*)$ state. The minimum of the surface crossing seam between the $^1(n\pi^*)$ and $^3(\pi\pi^*)$ states, designated as $^1(n\pi^*)/^3(\pi\pi^*)$-**SC**, was successfully optimized in the vicinity of the $^1(n\pi^*)_{min}$ state. The conical intersection of the $^3(n\pi^*)$- and $^3(\pi\pi^*)$-state PESs, namely, $^3(n\pi^*/\pi\pi^*)$-**CI**, was obtained as well, with the characteristic of having the average bond length of the minima of the two related states.

Key points involved in path A are as follows: The cleavage of the C1—C5 bond leads to an intermediate state, **A-INT**. The geometry of the **A-INT**-$^3(\pi\pi^*)_{min}$ state is quite similar to that of the ground state. Subsequently, **A-INT** undergoes a methyl migration through a transition state, denoted as **A-TS**, finally yielding the product **A-P**. With the methyl migration from C6 to C1, the bond length of C1—C6 decreases from 1.522 Å in **A-INT** to 1.436 Å in **A-TS**; the difference reaches 0.088 Å in the

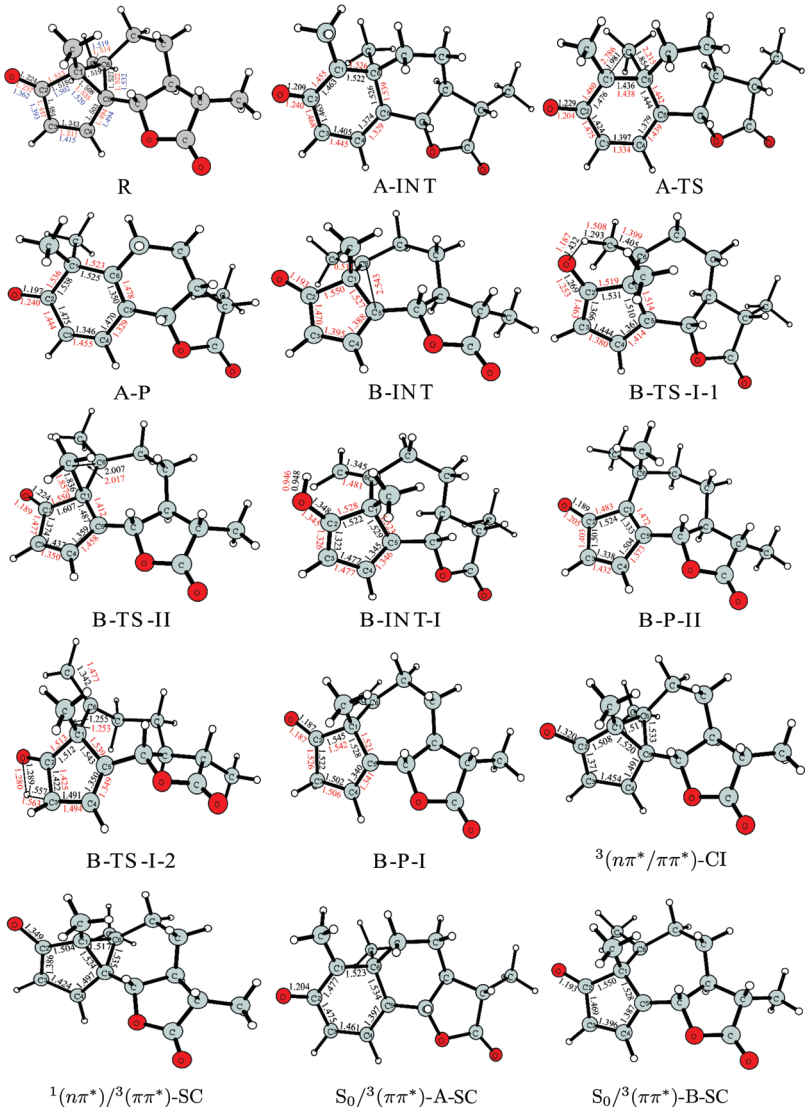

Figure 2. Selected optimized geometric parameters of critical points along the reaction pathway [S_0 in black, $^3(\pi\pi)$ state in red and $^1(n\pi)$ state in blue].

$^3(\pi\pi^*)$ state. Furthermore, the C—C bond length of the benzophenone moiety is equalized in the ground state for **A-TS**. In the $^3(\pi\pi^*)$ state, the C3—C4 bond length is 1.334 Å characterized by a double-bond property. As **A-P** is formed, the C2—C3, C3—C4, and C4—C5 bonds exhibit a single- and double-bond alternation character. The lowest surface crossing is located around **A-INT**, designated as $S_0/^3(\pi\pi^*)$-**A-SC**, with the characteristics of having equalized geometrical parameters in both **A-INT**-S_0 and **A-INT**-$^3(\pi\pi^*)_{min}$.

Key points involved in path B are as follows: Along with the augmentation of the distance between C5 and C6, the diradical intermediate **B-INT** in the $^3(\pi\pi^*)$ state was successfully optimized. A minimum in the ground state was not found, but we nevertheless optimized a surface crossing around **B-INT** with a geometry quite identical to that of the $^3(\pi\pi^*)$ state. The reaction pathway suggested in the experimental work of ref 6 contains successive steps with hydrogen abstraction from a methyl group to the adjacent oxygen of the ketone group to generate an intermediate in enol form, namely, **B-INT-I**, passing through the transition state **B-TS-I-1**. The C6—C7 (in the methyl group), C1—C2, and C4—C5 bond lengths in **B-TS-I-1** are shortened by 0.112, 0.031, and 0.026 Å, respectively, compared with those in **B-INT** in the $^3(\pi\pi^*)$ state. The enolic group in **B-INT-I** is ketonized, yielding the product **B-P-I** through a transition state denoted as **B-TS-I-2**. In each species, the equilibrium geometry of the five-membered alkyl ring in the ground state is quite similar to that in the $^3(\pi\pi^*)$ state. The notable diversity of the two states appears in the bond length of the newly formed vinyl fragment. The increased bond distance arises from the two singly occupied orbitals on the vinyl carbon atoms separately in the $^3(\pi\pi^*)$ state. In competition with the reaction pathway derived from hydrogen migration, another reaction channel might exist that involves a methyl-group shift. Therefore, **B-INT** undergoes a transition state, denoted as **B-TS-II**, leading to another product, called **B-P-II**. Along this reaction pathway, C1 is sp^3-rehybridized in **B-P-I**, and the distance between C1 and C6 increases. A minimum of the surface crossing is found adjacent to **B-INT**, denoted as $S_0/^3(\pi\pi^*)$-**B-SC**, and is quite identical to **B-INT**-$^3(\pi\pi^*)_{min}$. To provide a general overview of the multistep photoinduced reaction, the relative energies of the stationary points on the ground- and excited-state PESs are summarized in the Figure 3.

dx.doi.org/10.1021/jp203369b |*J. Phys. Chem. A* 2011, 115, 7815–7822

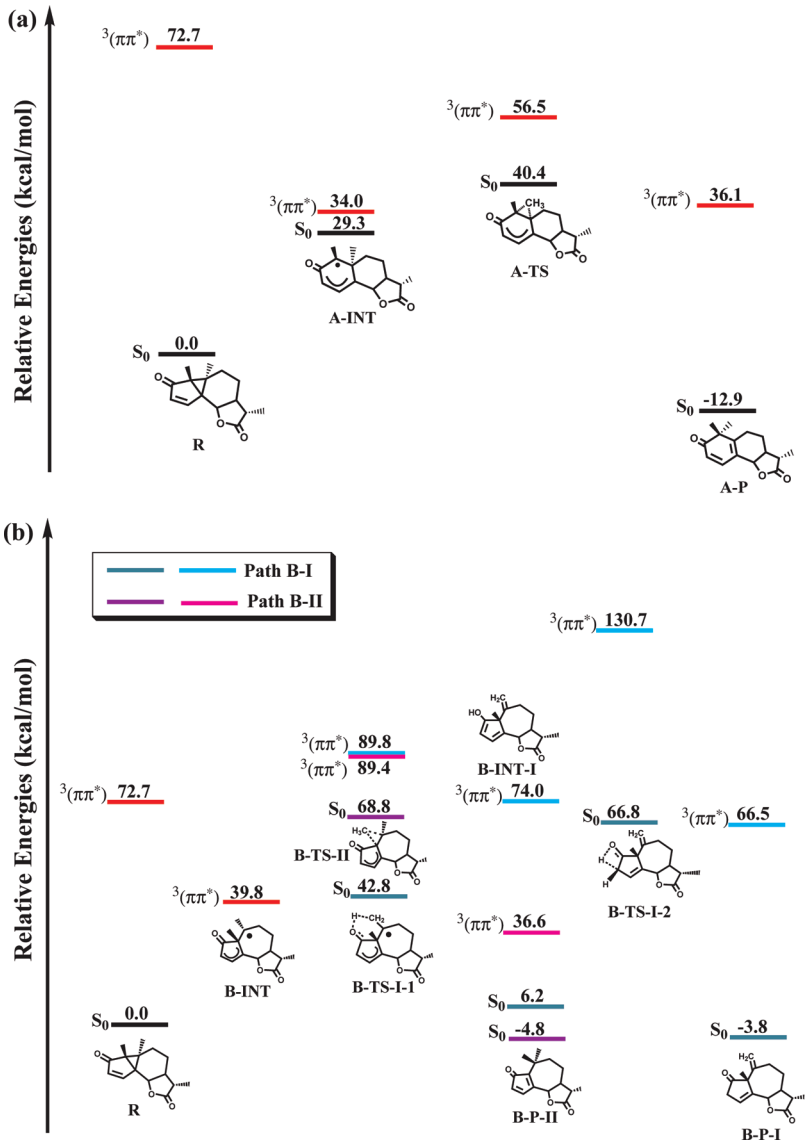

Figure 3. Energy levels of stationary points on the adiabatic PESs of the ground and excited states relevant to (a) path A and (b) path B.

Table 1. Vertical Excitation Energies (in eV) and Transition Assignments of Low-Lying Excited States of the Reactant at the CASPT2 level

state	transition	CASPT2	f	exp
$^1(n\pi^*)$	$n_o \rightarrow \pi^*$	3.52	0.001	3.70[a]
$^1(\pi\pi^*)$	$\pi \rightarrow \pi^*$	4.87	0.020	
$^3(n\pi^*)$	$n_o \rightarrow \pi^*$	3.32		
$^3(\pi\pi^*)$	$\pi \rightarrow \pi^*$	3.56		

[a] See ref 5.

Vertical Excitation Energies. Because the low-lying excited states of lumisantonin trigger successive reactions under the irradiation of UV light, we investigated the vertical energies, transition properties, and oscillator strengths at the CASPT2 level. They are collected in Table 1, along with relevant experimental values. The first singlet excited state is assigned to the $^1(n\pi^*)$ state arising from an oxygen lone pair to the π^*-type orbital at the C═O group with an energy of 3.52 eV, in good accord with experimental observation.[5] Its oscillator strength is as small as 0.001. The second singlet excited state lies above the $^1(n\pi^*)$ state, with a large oscillator strength corresponding to the strong band in the experimental absorption spectrum. However, promotion to the $^1(\pi\pi^*)$ state is not possible because of the unaffordable electronic transition energy under the given light wavelength of about 320 nm. The $^3(\pi\pi^*)$ state is the lowest triplet state and is ascribed to the promotion of a π-type bonding orbital mixed with the σ orbital along the C1—C5 and C5—C6 bonds to the π^*-type antibonding orbital in the cyclopentenone moiety. Its vertical transition energy is predicted to be 3.56 eV, as

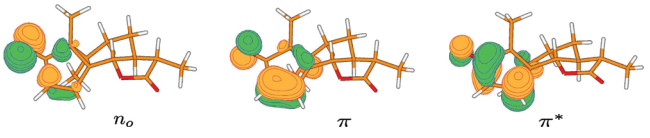

Figure 4. Molecular orbitals related to electronic promotion in the low-lying excited states.

Table 2. Relative CASPT2 Energies of the Reactions (in eV) and SOC Constants (SOCCs) of Surface Crossings (in cm^{-1})

	$\Delta E^{\ddagger}$		ΔE			
reaction	S_0	$^3(\pi\pi^*)$	S_0	$^3(\pi\pi^*)$	SC	SOCCs
			Path A			
R → A-INT	–	–	29.3	−38.7	$^1(n\pi^*)/^3(\pi\pi^*)$-**SC**	60.9
A-INT → A-P	11.1	22.5	−42.2	2.1	$S_0/^3(\pi\pi^*)$-**A-SC**	0.54
			Path B			
R → B-INT-I	42.8	–	6.2	–	$S_0/^3(\pi\pi^*)$-**B-SC**	0.43
R → B-INT	–	–	–	−32.9		
B-INT → B-INT-I	–	50.0	–	34.2		
B-INT-I → B-P-I	60.6	56.7	−10.0	−7.5		
R → B-P-II	68.8	–	−4.8	–		
B-INT → B-P-II	–	49.6	–	−3.2		

it is higher than the $^3(n\pi^*)$ state. The critical molecular orbitals related to electron promotion in the low-lying excited states are plotted in Figure 4.

Reaction Pathway on the Singlet Ground-State PES. As the reaction proceeds along path A, the rearrangement process occurs in a stepwise fashion on the adiabatic singlet ground-state PES. The first-step reaction gives rise to the intermediate species **A-INT** with no barrier, where the σ-bond rupture results in the separation of an electron pair. An electron population analysis of **A-INT** indicates that unpaired electrons are partially localized on the carbon of the methyl group bonding to C6 and distributed over the π-type orbital of the six-membered alkyl ring. Through a transition state of **A-TS**, **A-INT** successively leads to a methyl-group migration, finally yielding **A-P**.

The first-step reaction from **R** to **A-INT** is predicted to be endoergic by 29.3 kcal mol^{-1}. We attempted to search for a saddle point connecting **R** with **A-INT** by means of the restricted optimization methodology along the bond rupture direction. However, the energy was found to rise monotonically because of the sole involvement of bond breaking, and the reaction proceeds directly to the biradical metastable **A-INT**. The subsequent methyl migration from **A-INT** to **A-P** through **A-TS** is calculated to be exoergic by 42.2 kcal mol^{-1}, involving an energy barrier of 11.1 kcal mol^{-1}. Overall, the reaction taking place on the ground state is exothermic by 12.9 kcal mol^{-1}.

The other possible reaction channel, path B, features a stepwise mechanism as well. We could not find a stationary point on the singlet ground-state PES as an intermediate resulting from carbon bond rupture, but two transition states featuring bond breaking combined with hydrogen shift or methyl-group migration were successfully optimized. We found two distinct reaction pathways, named path B-I and path B-II. Through the transition state **B-TS-I-1**, an enolic intermediate is formed. The subsequent reaction involving ketonization yields **B-P-I** formation. The other reaction channel leads to **B-P-II** formation through **B-TS-II**.

From **R** to **B-INT-I**, the reaction is endoergic by 6.2 kcal mol^{-1} and needs to overcome an energy barrier as high as 42.8 kcal mol^{-1}. The subsequent hydrogen rearrangement from **B-INT-I** to **B-P-I** is predicted to be exoergic by 10.0 kcal mol^{-1}, with an energy barrier as high as 60.6 kcal mol^{-1}. In comparison, the methyl-group migration needs much more energy to overcome the substantially higher energy barrier of 68.8 kcal mol^{-1}

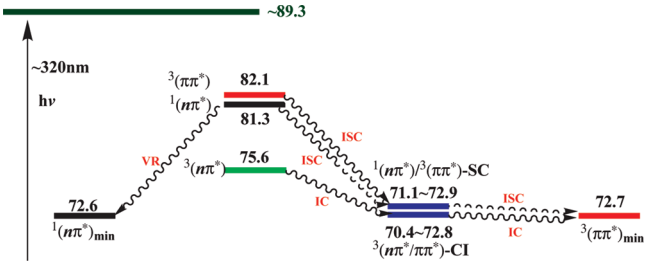

Figure 5. Excited-state decay channels in the Franck−Condon region (in kcal mol^{-1}).

and yields the product **B-P-II** along with the release of 6.2 kcal mol^{-1}. Evidently, path B-I predominates over path B-II dynamically. The computational results indicate that the thermal reaction from **R** to all products would not occur except under extremely high temperatures. The reaction energy changes of each reaction step on the ground-state PES are listed in Table 2.

Reaction Pathway on the Excited-State PES. To investigate the photolytic reaction mechanism from the reactant to the products on the excited-state PESs, we evaluated all of the energies of the stationary points, as well as the essential surface crossings relevant to the radiationless decay channels along the reaction pathway at the CASPT2 level. When exposed to irradiation light with a wavelength of about 320 nm, the electronic state of lumisantonin is excited from the singlet ground state to the first singlet excited state $^1(n\pi^*)$ assigned to the promotion of a lone-pair electron to the π^* orbital of C═O group. The vertical energy was calculated to be 81.3 kcal mol^{-1}, which can be matched with the irradiation energy and which is exoergic by 8.7 kcal mol^{-1}, relaxing to reach a minimum on the $^1(n\pi^*)$-state PES. Around the $^1(n\pi^*)_{min}$ state, we found a lowest-energy point on the seam of the $^1(n\pi^*)$- and $^3(\pi\pi^*)$-state PESs crossing. Upon further investigation of the significant crossing point, the SOC constant appeared to be as large as 60.9 cm^{-1}, indicating that there is an efficient radiationless channel through $^1(n\pi^*)/^3(\pi\pi^*)$-**SC** for the deactivation from the $^1(n\pi^*)$ state to the $^3(\pi\pi^*)$ state. The $^1(n\pi^*)_{min}$ and $^3(\pi\pi^*)_{min}$ states were found to be nearly degenerate, differing by only 0.1 kcal mol^{-1}. Although we did not find the $^3(n\pi^*)_{min}$ state near to the FC region, the conical intersection between the $^3(\pi\pi^*)$ and $^3(n\pi^*)$ states was optimized, suggesting that the IC process effectively takes place through $^3(n\pi^*/\pi\pi^*)$-**CI**. The radiationless decay channels from

dx.doi.org/10.1021/jp203369b |J. Phys. Chem. A 2011, 115, 7815–7822

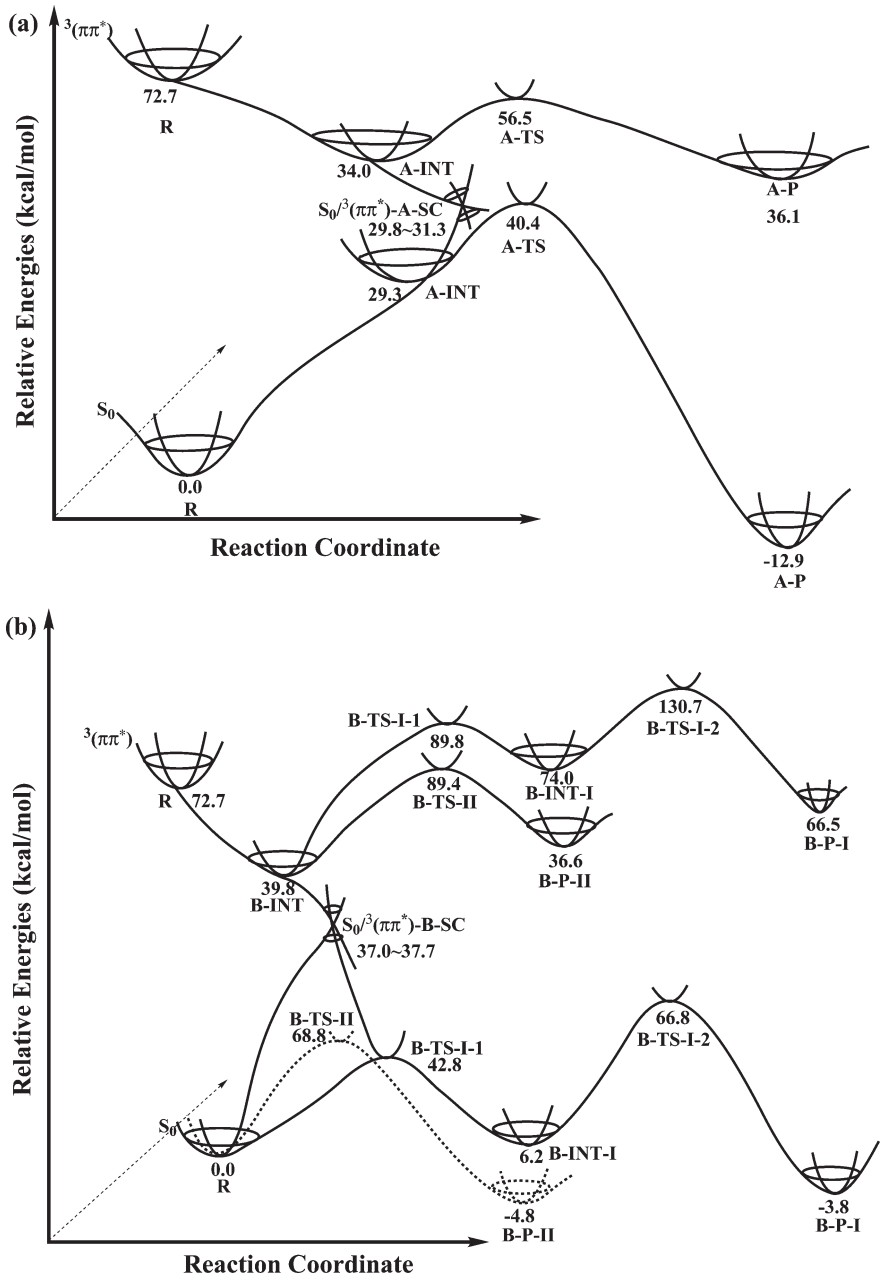

Figure 6. Energy levels of stationary points on the nonadiabatic PESs of the ground and excited states relevant to (a) path A and (b) path B.

the excited-state FC region to the stationary point on each excited-state PES are schematically described in Figure 5. Here, we list a range from the lower-state energy to the upper-state energy at the crossing point. As shown in Figure 4, promotion of an electron from π to π^* leads to electron rearrangement involving the σ orbital of the C—C bond. On the contrary, the electron transition from n_O to π does not greatly affect the change of electron density in the C—C σ orbital. Accordingly, we focus on the investigation of the photorearrangement pathway on the $^3(\pi\pi^*)$-state PES.

As displayed in Figure 3, the photolytic rearrangement on the lowest triplet-state PES is well-characterized as a stepwise reaction. Proceeding along path A on the $^3(\pi\pi^*)$-state PES, the first-step reaction involving the cleavage of the C1—C5 bond directly leads to **A-INT** as a biradical, by energy release of 38.7 kcal mol^{-1} with a free energy barrier. **A-INT**-$^3(\pi\pi^*)_{min}$ is a biradical similar to **A-INT**-S_0 in electron population. The methyl migration from **A-INT** to **A-P** through **A-TS** is endoergic by 2.1 kcal mol^{-1}, involving an energy barrier of 22.5 kcal mol^{-1}. In the region of **A-INT**, we successfully located an essential minimum of the surface crossing seam related to the ground- and $^3(\pi\pi^*)$-state PESs. The evaluated energy of $S_0/^3(\pi\pi^*)$-**A-SC** at the CASPT2 level shows that it lies below the $^3(\pi\pi^*)_{min}$ state by 2.7−4.2 kcal mol^{-1}, and the predicted SOC constant is 0.54 cm^{-1}.

The cleavage of the C5—C6 bond leads to path B on the $^3(\pi\pi^*)$-state PES. Following the track of the relative energy change with the increase of the distance between C5 and C6, the energy drops without any turning point, indicating that it is a barrier-free reaction. The C5—C6 bond rupture gives rise to the formation of **B-INT**-$^3(\pi\pi^*)_{min}$ with an energy release of

32.9 kcal mol^{-1}. The theoretical calculation predicts the following reaction along path B-I through a transition state **B-TS-I-1** featured by a hydrogen from a methyl group bonding to C6 and the oxygen bonding to C2. This step to the formation of **B-INT-I** is endoergic by 34.2 kcal mol^{-1}, with an energy barrier as high as 50.0 kcal mol^{-1}. Similarly, the saddle point linking **B-INT** with **B-P-II** is located slightly below **B-TS-I-1** by 0.4 kcal mol^{-1}. As **B-P-II** is formed, it releases an energy of 3.2 kcal mol^{-1} relative to **B-INT**. The whole reaction to **B-P-II** on the excited triplet-state PES is exoergic by 36.1 kcal mol^{-1}. The successive reaction from **B-INT-I** to **B-P-I** is characterized by an enol structure that must overcome an energy barrier as large as 56.7 kcal mol^{-1} to complete the ketonization reaction by release of 7.5 kcal mol^{-1}. The whole reaction is exothermic, with an energy release as large as 6.2 kcal mol^{-1}. The lowest point on the seam of the surface crossing between the $^3(\pi\pi^*)$-state PES and the singlet ground-state PESs, labeled $S_0/^3(\pi\pi^*)$-**B-SC**, lies 2.1−2.8 kcal mol^{-1} below **B-INT**-$^3(\pi\pi^*)_{min}$, and the SOC constant is predicted to be 0.43 cm^{-1}. All of the reaction energy changes along the reaction pathway on the $^3(\pi\pi^*)$-state PES and SOC constants of critical surface crossings are collected in Table 2.

Favorable Rearrangement Reaction Pathway. To illustrate the reaction mechanism of the rearrangement occurring on both the S_0- and $^3(\pi\pi^*)$-state PESs, the nonadiabatic reaction pathway from lumisantonin to each product is schematically represented in Figure 6. We found that the experimental wavelength of 320 nm gives an excitation to the first singlet excited state, $^1(n\pi^*)$, of lumisantonin with a non-negligible oscillator strength in the FC region. Subsequently, it can relax to the lowest stationary point on the $^1(n\pi^*)$-state PES and successively undergo a radiationless decay to the $^3(\pi\pi^*)$ state through $^1(n\pi^*)/^3(\pi\pi^*)$-**SC**, where an efficient decay channel appears as the result of a large SOC constant. Another conical intersection, $^3(n\pi^*/\pi\pi^*)$-**CI**, indicates a significant probability for the excited triplet-state conversion. In consideration of the dynamic dominance of the $^3(\pi\pi^*)$ state at the initial reaction step, we emphasize the following investigation of the reaction mechanism proceeding along the ground- and $^3(\pi\pi^*)$-state PESs.

Proceeding along path A the following steps occur: The C1—C5 bond rupture ascribed to promotion of an electron from the π orbital mixed with the σ orbital along the C1—C5 bond to the π^* orbital results in the formation of **A-INT**-$^3(\pi\pi^*)_{min}$. It is predicted to be a barrier-free reaction with an energy liberation of 38.7 kcal mol^{-1}. In the region of **A-INT**, the presence of the lowest surface crossing, $S_0/^3(\pi\pi^*)$-**A-SC**, indicates a possible decay channel from the $^3(\pi\pi^*)$ state to the ground state. Once the system has decayed to **A-INT**-S_0, it needs to surmount an energy barrier of 11.1 kcal mol^{-1} to yield **A-P**-S_0 lying 12.9 kcal mol^{-1} below **R**-S_0; otherwise, it needs to overcome the energy barrier by 22.5 kcal mol^{-1} leading to **A-P** on the $^3(\pi\pi^*)$-state PES.

Compared with the cleavage of the C1—C5 bond, the C5—C6 bond rupture leads to the other distinct reaction pathway, path B. Under light irradiation, C5—C6 bond cleavage takes place on the $^3(\pi\pi^*)$-state PES. Similarly to the initial photoinduced reaction along the path A, there is no energy barrier from **R**-$^3(\pi\pi^*)_{min}$ to **B-INT**-$^3(\pi\pi^*)_{min}$ lying 5.8 kcal mol^{-1} above **A-INT**-$^3(\pi\pi^*)_{min}$. The minimum of the surface crossing seam, $S_0/^3(\pi\pi^*)$-**B-SC** adjacent to **B-INT**-$^3(\pi\pi^*)_{min}$, suggests that the ISC process takes place after many molecular vibrations of **B-INT**-$^3(\pi\pi^*)_{min}$. In the absence of a stationary point of **B-INT** on the ground state, **B-INT**-$^3(\pi\pi^*)_{min}$ could either relax to **R**-S_0 with an energy release or overcome a relatively small energy barrier of around 5.0 kcal mol^{-1} to give **B-INT-I**-S_0. This reaction channel can be regarded as a dynamically favorable pathway compared with the other reaction pathway yielding **B-P-II**, after decay to the ground state. Subsequently, the reaction from **B-INT-I**-S_0 through a quite high energy barrier of 60.6 kcal mol^{-1} to **B-P-I** is exoergic by 10.0 kcal mol^{-1}. Assuming that the reaction occurs on the $^3(\pi\pi^*)$-state PES, the formation of **B-P-II** through methyl migration is favored by thermodynamics, whereas **B-P-I**-$^3(\pi\pi^*)_{min}$ can not be yielded through a ketonization reaction because the required energy is far beyond that corresponding to the initial irradiation wavelength. Overall, from the viewpoints of both thermodynamics and dynamics, path A is the favorable reaction pathway in the photoinduced rearrangement of lumisantonin, a conclusion that is consistent with the experimental observation.[6] On the other hand, pyrolysis of lumisantonin involves only the ground-state reaction pathway, leading to a different result than suggested by experiment. The theoretical studies here provide a basis to the understanding the reaction mechanism. Assuming path A on the ground-state PES, the cleavage of the C1—C5 bond is endoergic by 29.3 kcal mol^{-1}, with a free energy barrier from **R** to **A-INT** as a less stable intermediate. Accordingly, it the system can revert to **R**. In comparison with path A, the initial reaction of path B involves C5—C6 bond rupture together with a hydrogen migration, leading to that stable intermediate **B-INT-I**, which can undergo a ketonization reaction to finally yield **B-P-I**. Owing to the formation of the stable intermediate **B-INT-I**, path B is predominant over path A at high temperatures.

CONCLUSIONS

In this work, we carried out theoretical studies on the rearrangement reaction mechanism on the singlet ground-state and low-lying excited-state PESs using the CASSCF//CASPT2 method. Exposed to light with a wavelength of 320 nm, the accessible low-lying singlet state is the $^1(n\pi^*)$ state, which undergoes an effective nonradiative decay to the $^3(\pi\pi^*)$ state through a minimum of the surface crossing seam. Successive calculations indicated that the $^3(\pi\pi^*)$ state, ascribed to the promotion of an electron from the π orbital coupled to the C—C σ orbital in the three-membered alkyl ring to the π orbital localized on the conjugation carbon atoms, plays a critical role in the C—C bond cleavage leading to the subsequent stepwise reaction. According to the different C—C bond cleavages, the reaction pathway can be divided into two distinct types, labeled path A and path B. Path A arises from C1—C5 bond rupture featuring a barrier-free reaction on both the ground- and $^3(\pi\pi^*)$-state PESs and is favorable because of the dynamic and thermodynamic preferences on the triplet excited-state PES. Around **A-INT**, there possibly exists a deactivation decay channel from the $^3(\pi\pi^*)$ state to the ground state. Once having undergone the radiationless transition, the system could recover to lumisantonin by means of C1—C5 bond formation with an energy release. Alternatively, the excited lumisantonin in the $^3(\pi\pi^*)$ state could surmount an energy barrier to complete the reaction. Path B, derived from the cleavage of the C5—C6 bond, feasibly takes place on the ground-state PES because of the relatively high stability of the intermediates compared to **A-INT**-S_0. There also exists a decay channel from the $^3(\pi\pi^*)$ state to the ground state in the vicinity of **B-INT**, resulting in that subsequent reaction taking place on the ground-state PES. The initial step is a characteristic of a concerted reaction involving bond rupture and a hydrogen or methyl migration together on the ground-state PES. Owing to the much lower energy barrier compared to the methyl-migration reaction,

the channel leading to **B-INT-I** in enol form predominates on the ground-state PES.

AUTHOR INFORMATION

Corresponding Author
*E-mail: agren@theochem.kth.se (H.A.), zxcao@xmu.edu.cn (Z.C.).

ACKNOWLEDGMENT

This work was supported by a grant from the Swedish Infrastructure Committee (SNIC) for the project "Multiphysics Modeling of Molecular Materials", SNIC 022/09-25, as well as by the National Science Foundation of China (20733002 and 20873105) and the Ministry of Science and Technology (2011CB808504).The authors acknowledge Dr. Shilv Chen and Dr. Rongzhen Liao for providing some good suggestions.

REFERENCES

(1) Arigoni, D.; Bosshard, H.; Bruderer, H.; Büchi, G.; Jeger, O.; Krebaum, L. J. Photochemische Reaktionen. 2. Mitteilung ber gegenseitige Beziehungen und Umwandlungen bei Bestrahlungsprodukten des Santonins. *Helv. Chim. Acta* **1957**, *40*, 1732.

(2) Fisch, M. H.; Richards, J. H. The Mechanism of the Photoconversion of Santonin. *J. Am. Chem. Soc.* **1963**, *85*, 3029.

(3) Chapman, O. L.; Englert, L. F. A Mechanistically Significant Intermediate in the Lumisantonin to Photosantonic Acid Conversion1. *J. Am. Chem. Soc.* **1963**, *85*, 3028.

(4) Barber, L.; Chapman, O. L.; Lassila, J. D. Photochemical transformations. XXVII. Low-temperature photochemistry of umbellulone and lumisantonin. *J. Am. Chem. Soc.* **1968**, *90*, 5933.

(5) Fisch, M. H.; Richards, J. H. Photoproducts from irradiation of lumisantonin in aprotic medium. *J. Am. Chem. Soc.* **1968**, *90*, 1553.

(6) Fisch, M. H.; Richards, J. H. The mechanism of the photochemical rearrangement of lumisantonin. *J. Am. Chem. Soc.* **1968**, *90*, 1547.

(7) Schuster, D. I.; Fabian, A. C. The nature of quenching of ketone excited states using high concentrations of dienes. The reactive electronic excited state of [alpha]-santonin. *Tetrahedron Lett.* **1968**, *9*, 1301.

(8) Sasaki, T.; Eguchi, S. Reactions of isoprenoids. III. 1,3-Dipolar and Diels−Alder cycloaddition reactivity of lumisantonin. *J. Org. Chem.* **1968**, *33*, 4389.

(9) Fisch, M. H. The photochemistry of santonin: Zwitterionic intermediates. *J. Chem. Soc. D* **1969**, 1472.

(10) Zimmerman, H. E.; Crumrine, D. S.; Doepp, D.; Huyffer, P. S. Organic photochemistry. XXXVIII. Photochemistry without light and the stereochemistry of the type A dienone rearrangement. *J. Am. Chem. Soc.* **1969**, *91*, 434.

(11) Caine, D.; Alejande, A. M.; Ming, K.; Powers, W. J. Photochemical rearrangements of bicyclic 6/5-fused cross-conjugated cyclohexadienones and related compounds. *J. Org. Chem.* **1972**, *37*, 706.

(12) Zimmerman, H. E.; Shorunov, S. Heterocyclic Photochemistry in Contrast with Carbon Behavior. Regioselective Photochemical Rearrangement of an Azacyclohexadienone: Mechanistic and Exploratory Organic Photochemistry. *J. Org. Chem.* **2009**, *74*, 5411.

(13) Roos, B. O. The Complete Active Space Self-Consistent Field Method and Its Applications in Electronic Structure Calculations. In *Advances in Chemical Physics: Ab Initio Methods in Quantum Chemistry*; John Wiley & Sons, Inc.: New York, 1987; Vol. 69, p 399.

(14) Hariharan, P. C.; Pople, J. A. The influence of polarization functions on molecular orbital hydrogenation energies. *Theor. Chim. Acta* **1973**, *28*, 213.

(15) Krishnan, R.; Binkley, J. S.; Seeger, R.; Pople, J. A. Self-consistent molecular orbital methods. XX. A basis set for correlated wave functions. *J. Chem. Phys.* **1980**, *72*, 650.

(16) Andersson, K.; Malmqvist, P.-Å.; Roos, B. O.; Sadlej, A. J.; Wolinski, K. Second-order perturbation theory with a CASSCF reference function. *J. Phys. Chem.* **1990**, *94*, 5483.

(17) Andersson, K.; Malmqvist, P.; Roos, B. O. Second-order perturbation theory with a complete active space self-consistent field reference function. *J. Chem. Phys.* **1992**, *96*, 1218.

(18) Dunning, T. H. Gaussian basis sets for use in correlated molecular calculations. I. The atoms boron through neon and hydrogen. *J. Chem. Phys.* **1989**, *90*, 1007.

(19) Frisch, M. J.; Trucks, G. W.; Schlegel, H. B.; Scuseria, G. E.; Robb, M. A.; Cheeseman, J. R.; Montgomery, J. A., Jr.; Vreven, T.; Kudin, K. N.; Burant, J. C.; Millam, J. M.; Iyengar, S. S.; Tomasi, J.; Barone, V.; Mennucci, B.; Cossi, M.; Scalmani, G.; Rega, N.; Petersson, G. A.; Nakatsuji, H.; Hada, M.; Ehara, M.; Toyota, K.; Fukuda, R.; Hasegawa, J.; Ishida, M.; Nakajima, T.; Honda, Y.; Kitao, O.; Nakai, H.; Klene, M.; Li, X.; Knox, J. E.; Hratchian, H. P.; Cross, J. B.; Bakken, V.; Adamo, C.; Jaramillo, J.; Gomperts, R.; Stratmann, R. E.; Yazyev, O.; Austin, A. J.; Cammi, R.; Pomelli, C.; Ochterski, J. W.; Ayala, P. Y.; Morokuma, K.; Voth, G. A.; Salvador, P.; Dannenberg, J. J.; Zakrzewski, V. G.; Dapprich, S.; Daniels, A. D.; Strain, M. C.; Farkas, O.; Malick, D. K.; Rabuck, A. D.; Raghavachari, K.; Foresman, J. B.; Ortiz, J. V.; Cui, Q.; Baboul, A. G.; Clifford, S.; Cioslowski, J.; Stefanov, B. B.; Liu, G.; Liashenko, A.; Piskorz, P.; Komaromi, I.; Martin, R. L.; Fox, D. J.; Keith, T.; Al-Laham, M. A.; Peng, C. Y.; Nanayakkara, A.; Challacombe, M.; Gill, P. M. W.; Johnson, B.; Chen, W.; Wong, M. W.; Gonzalez, C.; Pople, J. A. *Gaussian 03*; Gaussian, Inc.: Wallingford, CT, 2004.

(20) Werner, H.-J.; Knowles, P. J.; Lindh, R.; Manby, F. R.; Schütz, M.; Celani, P.; Korona, T.; Rauhut, G.; Amos, R. D.; Bernhardsson, A.; Berning, A.; Cooper, D. L.; Deegan, M. J. O.; Dobbyn, A. J.; Eckert, F.; Hampel, C.; Hetzer, G.; Lloyd, A. W.; McNicholas, S. J.; Meyer, W.; Mura, M. E.; Nicklass, A.; Palmieri, P.; Pitzer, R.; Schumann, U.; Stoll, H.; Stone, A. J.; Tarroni, R.; Thorsteinsson, T. *Molpro, A Package of Ab Initio Programs*, version 2006.1; University College Cardiff Consultants Limited: Cardiff, U.K., 2006; see http://www.molpro.net.

(21) Karlström, G.; Lindh, R.; Malmqvist, P.-Å.; Roos, B. O.; Ryde, U.; Veryazov, V.; Widmark, P.; Cossi, M.; Schimmelpfennig, B.; Neogrady, P.; Seijo, L. MOLCAS: A program package for computational chemistry. *Comput. Mater. Sci.* **2003**, *28*, 222.